Smart Structures and Systems, *Vol. 29, No. 4 (2022) 535-547*
https://doi.org/10.12989/sss.2022.29.4.535

Effect of brittleness on the micromechanical damage and failure pattern of rock specimens

Mehrdad Imani, Hamid Reza Nejati*, Kamran Goshtasbi and Amin Nazerigivi

Rock Mechanics Division, School of Engineering, Tarbiat Modares University, Tehran, Iran

(*Received December 17, 2020, Revised December 19, 2021, Accepted December 23, 2021*)

Abstract. Failure patterns of rock specimens represent valuable information about the mechanical properties and crack evolution mechanism of rock. Several kinds of research have been conducted regarding the failure mechanism of brittle material, however; the influence of brittleness on the failure mechanism of rock specimens has not been precisely considered. In the present study, experimental and numerical examinations have been made to evaluate the physical and mechanical phenomena associated with rock failure mechanisms through the uniaxial compression test. In the experimental part, Unconfined Compressive Strength (UCS) tests equipped with Acoustic Emission (AE) have been conducted on rock samples with three different brittleness. Then, the numerical models have been calibrated based on experimental test results for further investigation and comparing the micro-cracking process in experimental and numerical models. It can be perceived that the failure mode of specimens with high brittleness is tensile axial splitting, based on the experimental evidence of rock specimens with different brittleness. Also, the crack growth mechanism of the rock specimens with various brittleness using discrete element modeling in the numerical part suggested that the specimens with more brittleness contain more tensile fracture during the loading sequences.

Keywords: acoustic emission; brittleness; failure pattern; micro-crack; spalling; splitting

1. Introduction

Rock engineering projects deal with different issues which should not be underestimated at any stages of project investigation such as the failure mechanism of rock. Failure modes of surface and underground excavations are closely related to the failure and crack evolution mechanism of rock specimens. Formerly, several researchers have conducted different projects related to the evaluation of rock failure behavior like failure mechanism of intact rock specimens, deformation mechanisms (Hoek and Bieniawski 1965, Bieniawski 1967, Wawersik and Fairhurst 1970, Bobet and Einstein 1998, Sagong and Bobet 2002, Mughieda and Khawaldeh 2006, Cai and Liu 2009, Park and Bobet 2009, Panaghi *et al*. 2015, Chen *et al*. 2017, Khodayar and Nejati 2018, Chen *et al*. 2020).

It should be noted that experimental examinations faced uncertain restrictions due to the essence of the micro-mechanical behavior of rock specimens. Using Acoustic Emission (AE) sensors to monitor the fracturing process of specimens during the loading sequences can be useful in this regard, although many aspects of this method particularly the number of cracks have remained uncertain. That means particle numerical modeling is a highly trustworthy method to assess micro- mechanical phenomena in rock specimens. In recent times, studies on the numerical simulation of the failure mechanism of rock specimens were managed by other researchers (Stefanov 2008, Wang *et al*. 2014, Imani *et al*. 2017, Mardalizad *et al*. 2018).

It is worthwhile mentioning that the crack evolution mechanism and fracturing process of rocks are significantly affected by the brittleness factor. Based on the definition, a brittle fracture is characterized by a nil or minimum plastic deformation, whereas ductile fracture is accompanied by a significant extent of plastic deformation Nejati and Moosavi (2017). There are three distinct stages through the failure process of intact rocks: (1) initiation of micro-cracks (2) propagation of micro-cracks and (3) micro-crack coalescence. These three stages are affected by brittleness, and consequently, control the entire failure and damage evolution mechanism of rocks. For the importance of the above-mentioned discussion, in the present study influence of brittleness on the failure mechanism of rock specimens was considered using experimental and numerical studies.

2. Rock brittleness

One of the most important inherent mechanical properties of rock is brittleness in association with intrinsic natural rock structure considerably impacting the failure process of rock. Despite diverse rock brittleness measurement methods, scientists have not reached a unique standard index to describe or measure the brittleness factor. The influence of brittleness on the mechanical properties of rock specimens has been considered by Hucka and Das (1974). Based upon their results, rock specimens with a high value of brittleness possess low-value plastic deformation and a high ratio of compressive to tensile

*Corresponding author, Ph.D.,
E-mail: h.nejati@modares.ac.ir

ISSN: 1738-1584 (Print), 1738-1991 (Online)

strength. Moreover, Kahraman (2002) has investigated the correlation between brittleness and drillability by using three different types of brittleness index ($B_1 = \frac{\sigma_c}{\sigma_t}, B_2 = \frac{\sigma_c+\sigma_t}{\sigma_c-\sigma_t}$, $B_3 = \frac{\sigma_c \times \sigma_t}{2}$). They suggested a strong exponential correlation among penetration rate of TBM, the brittleness of B_1 and B_2. Other researchers such as Kahraman and Altindag (2004) studied the effect of fracture toughness in this concern. They revealed a strong correlation between fracture toughness and $B_3(\frac{\sigma_c \times \sigma_t}{2})$, however, a significant relationship between fracture toughness and $B_2(\frac{\sigma_c+\sigma_t}{\sigma_c-\sigma_t})$ could not be sensed. Furthermore, Gong and Zhao (2007) used the ratio of uniaxial compression to Brazilian tensile strength as a brittleness index and showed the crushed zone and radial cracks increase with increasing of brittleness index. Heidari *et al*. (2014) examined the interconnection among three different types of brittleness index ($BI_1 = \frac{\sigma_c}{\sigma_t}$, $BI_2 = \frac{\sigma_c+\sigma_t}{\sigma_c-\sigma_t}$, $BI_3 = \frac{\sigma_c \times \sigma_t}{2}$) and porosity. They indicated that no correlation between the brittleness index values and the porosity values might be found; nevertheless, they showed that the values of these brittleness indices (BI_1, BI_2 and BI_3) reduced due to saturation. In addition, some empirical models for estimation of specific energy have been suggested by Dursun and Gokay (2016) as a result of the correlation between cuttability and brittleness. Meng *et al*. (2015) recommended two new brittleness indexes based on the stress-strain curve and the post-peak stress curve. These new indices could demonstrate the influence of confining pressure on rock brittleness according to the stress-strain curve.

Some of the recommended rock brittleness indices can be seen in Table 1. The symbols used in Table 1 were defined as follow: σ_c is uniaxial compression strength in MPa, σ_t is tensile strength in MPa, q is the percentage of fines formed in the Protodyakonov impact test S_{20} is the percentage of a rock sample that passes the 11.2 mm sieve after 20 drops of the weight in an impact test for TBM performance prediction in the NTNU model, and E is the elastic modulus of rock in GPa.

With respect to the significance of the brittleness index of rock, the key focus of the conducted investigation was to investigate the failure mechanism of rock using the ratio of uniaxial compression strength to Brazilian tensile strength since a quite number of investigations are directly related to the failure mechanism in the field of brittleness. This is a common index to evaluate rock brittleness because determination of the Uniaxial Compression Strength (UCS) and the Brazilian tensile strength (BTS) are the first steps in analyzing rock mechanical properties (Hucka and Das 1974, Kahraman 2002, Heidari *et al*. 2014, Nejati and Ghazvinian 2014, Meng *et al*. 2015).

Table 1 Some of the suggested brittleness indices

Proposed Brittleness Index (BI)	Reference
$BI = q\sigma_c$	Protodyakonov (1962)
$BI = \frac{\sigma_c}{\sigma_t}$	Hucka and Das (1974)
$BI = (\sigma_c - \sigma_t)/(\sigma_c + \sigma_t)$	Hucka and Das (1974)
$BI = S_{20}$	Blindheim and Bruland (1998)
$BI = \sigma_c\sigma_t/2$	Altindag (2000)
$BI = (\sigma_c\sigma_t)^{0.72}$	Yarali and Soyer (2011)
$BI = ({\sigma_t}^{0.84}E^{0.51})/{\sigma_c}^{0.21}$	Nejati and Moosavi (2017)

In the present study, it is intended to consider the role of brittleness in rock failure mechanism by means of different features including the ratio of UCS to BTS, the stress-strain curve, and the number of tensile and shear cracks. For this purpose, the Particle Flow Code 2-dimensional (PFC2D) software based on the Discrete Element Method (DEM) was used to examine the effect of brittleness on the failure behavior of rocks. Firstly, experimental tests were completed to achieve the macro-mechanical properties of intact rock. Secondly, an inverse-modeling approach was used to calibrate the rock micro-mechanical properties in order to receive the desired macro-parameters (experimental results) in numerical modeling. Finally, the validated numerical model was employed for further study of the mechanical behavior of rock specimens.

3. Failure pattern of rock specimens in uniaxial compression test

Rock strength can be simply experienced by the uniaxial compression test and this technique is commonly used in initial studies of different rock engineering developments. Various parameters might control the failure mode of rock specimens in the uniaxial compression test (Fakhimi and Hemami 2015, Gao *et al*. 2021). Therefore, perceiving the behavior and mechanism of failure thoroughly in brittle materials such as rock and concrete is highly complicated and the failure pattern is known to be extremely complex. Crack propagation in rocks is inherently uncertain in comparison to crack propagation in homogenous materials such as metals, due to their intricate matrix-including various micro-cracks, heterogeneity, anisotropy, and crystalline structure.

Micro-cracks, damage zone, and flaws are an inseparable part of material such as rocks (Jaeger *et al*. 2009, Marji 2014) and certainly have an impact on the failure mechanism of rocks because of stress concentration on the micro-crack tips (Ghazvinian *et al*. 2013, Marji 2015, Haeri and Marji 2016). However, other operative factors such as failure modes, failure pattern, thermal effect, scaled effect, and application of effective strength ratios have been continued to engage researchers. These parameters vary among different rock types considerably (Khodayar and Nejati 2018, Fan *et al*. 2020, 2021). In addition, failure mechanism and microstructural behavior are heavily influenced by loading rate because rock samples show a completely different failure mechanism by increasing the strain rate. (Cai *et al*. 2007, Fan *et al*. 2017, Asadizadeh *et al*. 2021).

Numerous studies were conducted to investigate the effect of different parameters on failure modes of specimens

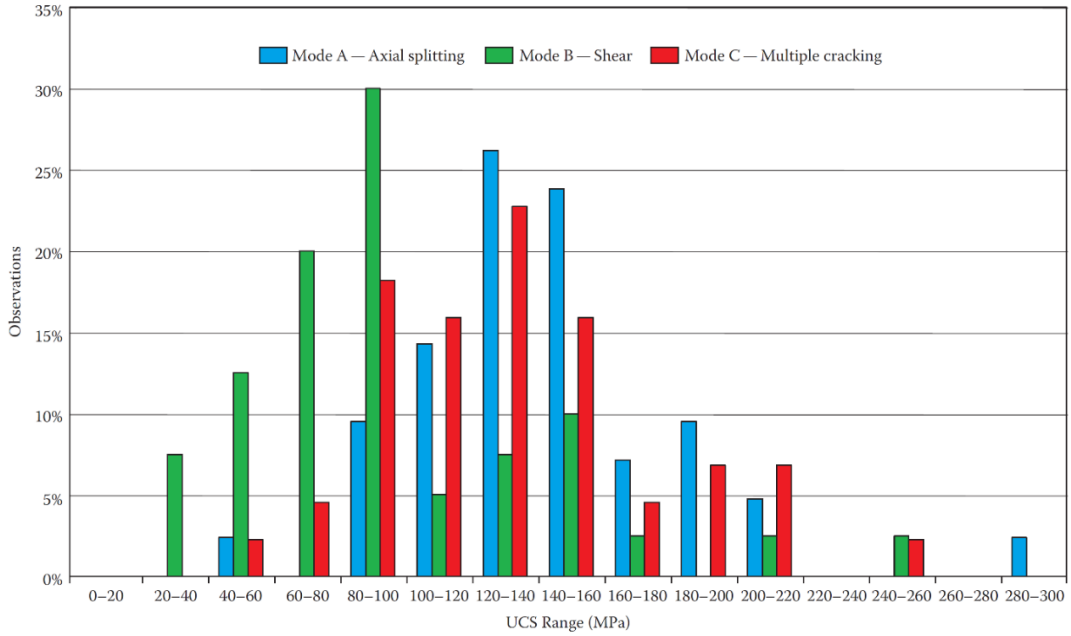

Fig. 1 Frequency of the observed failure modes in various range of UCS (Villaescusa 2014)

under uniaxial compression. Paul (1968) documented three failure modes of (1) splitting, (2) shearing, and (3) spalling for heterogeneous materials under uniaxial compression loading.

Gramberg (1989) identified two main classes of (1) axial cleavage and (2) conjugate shear for brittle rock specimen subjected to uniaxial compression. Szwedzicki and Shamu (1999) evaluated effects of strength on failure modes of rock samples and recognized five dissimilar modes of failure for cylindrical specimens under uniaxial compression loading as (1) simple extension, (2) multiple extension, (3) multiple fracturing, (4) multiple shear and (5) simple shear. Basu *et al*. (2013) analyzed the failure modes of granite, schist, and sandstone under uniaxial compression tests regarding corresponding strengths and observed six different failure modes of (1) axial splitting, (2) shearing along a single plane, (3) double shearing, (4), multiple fracturing, (5) along foliation, and (6) Y shaped failure.

Villaescusa (2014) evaluated a significant amount of data regarding the uniaxial compression test and showed that the macro-failure modes of isotropic rock specimens in the uniaxial compression test are: (1) axial splitting (2) shearing, and (3) multiple cracking. Also, results presented that a wide range of uniaxial compressive strength values may be obtained for each failure mode Fig. 1. As it can be seen in Fig. 1, UCS is not a meaningful parameter for discrimination of the macro-failure modes in the uniaxial compression test.

4. Experimental study

Macro-failure modes of rock specimens are heavily influenced by the induced micro-cracks during the loading sequences. Nejati and Ghazvinian (2014) showed that an increase in rock brittleness increases the frequency of induced micro-cracks, and the ratio of micro- to macro-crack density decreases with increasing rock brittleness. An experimental setup including a hydraulic testing machine with a data acquisition system was employed to determine the mechanical properties of samples through uniaxial compression tests and Brazilian tests. NX specimens (54 mm diameter) were prepared for the determination of the mechanical properties of rock specimens. The specimens with the length-to-diameter ratio of 2-2.5 were used and the loading rate was kept at 0.5 MPa/s in the uniaxial compression test. Besides, Brazilian disk specimens with the diameter-to-length ratio of 0.5-1 were prepared and the loading rate was kept at 0.2 kN/s in Brazilian test approach. Uniaxial compressive test and the Brazilian test were accomplished on the selected specimens and the failure patterns of the specimens detected.

4.1 Selection of rock samples

Several rock types with different brittleness were chosen to evaluate the effects of brittleness on the rock failure pattern. The tests were carried out in accordance with procedures suggested by International Society for Rock Mechanics on testing as uniaxial compression test and Brazilian test (ISRM 1981). The average values of compressive and tensile strength of tested specimens are listed in Table 2. The selected specimens can be categorized into three different of rock brittleness:

(1) Low-brittle: $BI < 9$
(2) Semi-brittle $9 \leq BI \leq 15$
(3) High-brittle $BI > 15$

4.2 Macro-failure patterns of Rock specimens under uniaxial compression

Macro-failure patterns of the tested specimens are illustrated in Figs. 2-4. As illustrated in Fig. 2, high-brittle specimens (BI>15) have shown the axial splitting failure

Table 2 Mechanical properties of the chosen rock specimens

Specimen types	σ_c (MPa)	σ_t (MPa)	$BI = \frac{\sigma_c}{\sigma_t}$	Failure mode
Grey Granite	224	10	22.40	Splitting
Black and White Granite	120	6.5	18.46	Splitting
Marble	139	8	17.38	Splitting
Sandstone	159.3	11.58	13.76	Shearing
Conglomerate	20.18	1.8	11.21	Shearing
Limestone	23.66	2.5	9.46	Shearing
Marl	21.63	3.25	6.65	Spalling - Shearing
Siltstone	18.6	2.2	8.45	Spalling - Shearing
Rock-like plaster	6.60	1	6.60	Spalling - Shearing

pattern. In these types of rocks, failure is occurred by the formation of vertical cracks. Fig. 3 shows the shearing failure mode, the most common of which can be observed in semi-brittle rock specimens ($9 \leq BI \leq 15$). These types of rocks show visible diagonal crack formation.

Also, low-brittle specimens (BI < 9) like marl and siltstone have spalling-shearing failure mode (Fig. 4). Spalling failure which includes the formation and propagation of tensile micro-cracks underneath the surface of specimens is usually accompanied by shear micro-cracks. Tensile micro-cracks were created in the first stages of loading, but the final failure mode is influenced by a large number of shear micro-cracks.

4.3 Crack evolution mechanism in rock specimens

The crack evolution mechanism of materials was investigated by the distribution of micro-cracks and their evolution in loading sequences (Ren *et al*. 2011). Initiation, propagation and coalescence of micro-cracks significantly affect the damage evolution and consequently macroscopic failure behavior of materials (Nejati and Ghazvinian 2014).

Acoustic emission (AE) is an appropriate technique for monitoring of crack evolution in materials due to elastic sound waves emitted from the material body after any deformation and crack propagation events. Indeed, fracturing and deformation of materials have initially resulted in the emission of elastic waves which propagate within the bulk of the material. Fig. 5 illustrates a typical AE signal indicating some key acoustic parameters for interpretation of physical and mechanical events corresponding to the cracking and failure of specimens

(a) Grey Granite (b) Black and White Granite (c) Marble

Fig. 2 Tensile axial splitting failure mode of high-brittle specimens

(a) Sandstone (b) Conglomerate (c) Limestone

Fig. 3 Shearing failure mode of semi-brittle specimens

(a) Marl (b) Siltstone (c) Rock-like plaster

Fig. 4 Spalling-shearing failure mode of low-brittle specimens

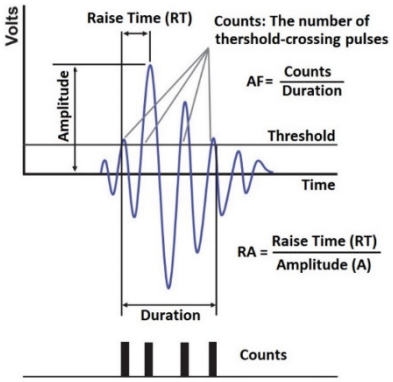

Fig. 5 AE parameters

under loading sequences. These parameters are described as follows:

Amplitude, A, is the highest value of the AE wave and can be reported in either voltage, (V) or decibels, (dB).

Threshold is the operator assumed value of amplitude, normally it is decided and set based on background noise.

AE Hit is a signal that surpasses the threshold and results a system channel to gather data.

AE counts indicate the number of times that an AE signal surpasses a distinct threshold during one AE signal.

AE energy represents the area under the amplitude - time curve and above the threshold value.

Rise Time (*RT*) is related to the time interval starting from the time of AE signal generation to the time of the signal achieving its maximum amplitude. *AE duration* states the time span from the starting point to the end point of the AE signal.

Moreover, two worthwhile parameters that can be deduced indirectly based on the AE signal are known as the Average Frequency (AF) and RA value. AF can be calculated from AE counts divided by duration, and RA value is Raise Time (RT) divided by amplitude. Tensile cracks usually produce acoustic signals with high frequency and low RA value while the waves emitted due to shear cracks have low frequency and high RA values (Aggelis *et al*. 2011). It should be noted that determination of a certain frequency and RA value for rock specimens to precisely distinguish the tensile and shear cracks from each other is not possible. However, increasing in the frequency and/or decreasing in RA value of AE signals indicate an increase in the number of tensile cracks in the specimens (Nejati *et al*. 2020, Khodayar and Nejati 2018).

Generally, the amplitude specifies the scale of induced crack, since small scale cracks emit waves with low amplitude, however, large scale cracks produce signals with higher amplitude. Also, the cumulative AE hits of the AE counts can successfully represent the number of induced cracks in different loading sequences.

In the present study, the AE technique was adopted to detect damages occurring in the experimental approach of rock samples subjected to variable stresses. As mentioned before to analyze the failure behavior, observed AE signals during the micro-structural cracking can be valuable. For evaluation of the micro-mechanical events in rock specimens, AE activities of three different rock samples from the three categories (high-brittle, semi-brittle, and low-brittle) under uniaxial compressive load were recorded and it can be seen in Fig. 6. The mechanical properties of these nominated samples were presented in Table 3.

As shown in Fig. 6, different AE's have been obtained from different rock samples. Three distinguished regions can be identified for cumulative AE counts of Granite, two regions for AE diagram of Sandstone and only one region was detectable in AE diagram of rock-like plaster.

The Kaiser effect which is used to approximate the sample's memorized stress can be defined as the changing slope of cumulative AE hits diagram versus stress. To evaluate the previous in situ stress condition in a case of memorized stress of sample, the inflexion point of the AE hits diagram should be referred. However, the present study discusses the effect of the brittleness and the fracturing process on the variation of AE counts versus applied stress.

Table 3 Mechanical properties of Granite, Sandstone and rock-like plaster

Rock types	UCS (MPa)	BTS (MPa)	E (GPa)	ν	$B = \frac{\sigma_c}{\sigma_t}$
Granite	224	10	60	0.2	22.4
Sandstone	159.3	11.58	39.63	0.17	13.74
Rock-like plaster	6.6	1	5	0.18	6.6

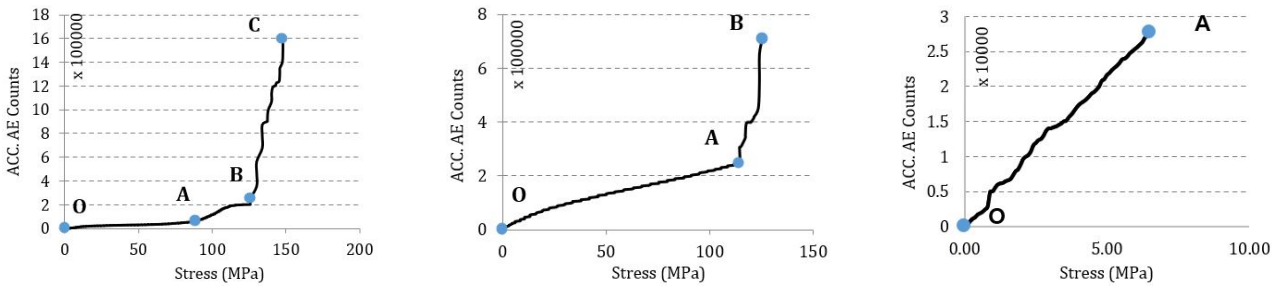

(a) Granite (b) Sandstone (c) Rock-like plaster

Fig. 6 Variation of cumulative AE counts of different rock types

As illustrated in Fig. 6, variations of cumulative AE hits versus stress for the three rock types are different from each other. It can be sensed that in the AE curves of the Granite sample, there are three dissimilar slope lines of O-A, A-B and B-C, however, there are two slope lines of O-A and A-B in the Sandstone AE curve. At the same time, only one slope line can be observed for rock-like plaster.

It should be noted that the inflection of the AE curve in Fig. 6(a) is not due to the Kaiser effect of the Granite sample, because the stress corresponding to the inflection points of Granite is 88, which is considerably more than the probable memorized stress for the studied rock samples. Accordingly, the most probable interpretation for the different slope lines in AE curves can be due to the mechanical properties of rock samples particularly rock brittleness.

Commonly, two sources are well documented for origination of AE signals from rock samples during loading, first, the frictional movement along the existing cracks, and second, crack initiation or propagation (Yoshikawa and Mogi 1981, Lavrov 2003, Nazerigivi *et al*. 2017). Based on these two phenomena, the rate of AE counts variation (change of slope in the diagram of cumulative AE hits versus stress) can be justified.

Flaws, cracks or heterogeneity are common in rock samples. Through a loading sequence, a frictional movement along the existing crack can be detected as a source of AE signals. Moreover, crack propagation which is characterized as another source of AE signals is affected by rock brittleness. In this regard, quick crack propagation by low energy discharge together with no significant plastic deformation belongs to brittle fracture, although ductile fracture is generally complemented by a considerable amount of plastic deformation. Meanwhile, more events are distinguishable in comparison to the low brittle rock sample during a certain time loading before total collapse based on the crack coalescence. Thus, a shifting slope line of AE counts versus stress is observed in brittle rocks (like Granite) which is not owed to the Kaiser effect (line A-B in Fig. 6(a)).

Based on the previous discussion, frictional movements generate more signals in semi-brittle and specifically low-brittle rock types compared to the brittle ones. With respect to this, the rate of AE events for low-brittle rock samples is more than the events emitted by high-brittle rocks at the start of the loading sequence.

It can be stated that rock brittleness affects the variation of cumulative AE signals versus stress regardless of the stress memory. The AE curve of low-brittle rock types displays one region; however, the AE curve of semi-brittle and high-brittle rock types enclose two and three regions, respectively.

The number of induced fractures in rock samples is another important parameter which is influenced by the rock brittleness. As shown in Fig. 6, the number of AE counts generated in Granite is more than the number of AE counts of Sandstone and rock-like plaster. This means that the frequency of induced fracture under monotonic loading in Granite is more than that in Sandstone and rock-like plaster.

More addition, the types of fractures are another important notion in the failure analysis of rock specimens. Aggelis *et al*. (2013) concluded that the events attributed to pure tensile fractures produce acoustic waves with higher frequency than the shear ones. The average frequency of the recorded hits from different specimens can be compared for studying the failure mechanism of rock specimens.

Fig. 7 illustrates the variation of average frequency with RA for the three rock types. For evaluation of the types of induced fractures for three studied specimens, all of the hits emitted from the rock specimens during the loading sequences were recorded. As shown in Fig. 7, the average frequency of the signals emitted from Granite is more than the average frequency of waves corresponding to Sandstone and rock-like plaster. Also, increasing in the value of RA is observable in the signals emitted from rock-like plaster compared to Sandstone and Granite. Therefore, it can be concluded that the rock with more brittleness contains more tensile fracture during the loading sequences.

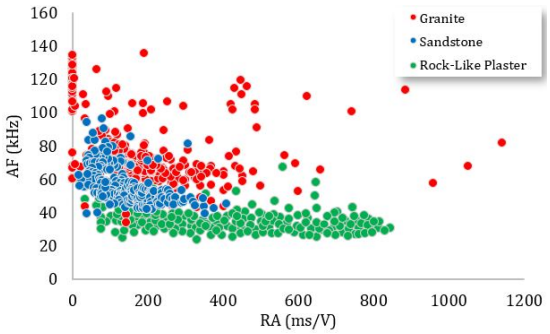

Fig. 7 Variation of average frequency with time for the three rock types

5. Numerical modelling

For more investigation, in this section, the three types of rock with various brittleness values (Table 3) were chosen and their micro-mechanical behaviors were investigated by means of numerical modelling. After doing experimental tests, the numerical models of them (rock-like plaster, Sandstone and Granite) were prepared using PFC2D.

Potyondy and Cundall (2004) proposed a Bonded Particle Model (BPM) for simulation of rock and rock-like materials based on DEM. The BPM is implemented in the two and three-dimensional (disk and ball) discontinuous programs PFC2D and PFC3D. The particles are assumed as rigid that they are allowed to be bonded together at their contacts points. Each particle can move and connect by rigid spring simulated by various bonding models. Newton's law is used in PFC software for the particles and force-displacement law of each contact. Also, rock can be modeled as a dense packing of cemented grains by contacts. The particles interact through normal and shear springs and the particles can transfer, rotate and change their positions according to forces and moments acting on their centers (Itasca 2008). One of the most essential advantages of the PFC is that the failure process including crack initiation, propagation, and coalescence can be simulated by breaking of contact bonds without any crack breakage criteria (Xu *et al*. 2016).

5.1 Bonding model in PFC

The PFC particles allowed to be bonded together at contact with different bonding models. Two early conventional bonded models supported in PFC are contact-bond model (CBM) and parallel-bond model (PBM) (Itasca 2008). Although the mechanical behavior of PBM for simulation of rocks is more reliable than CBM and it has been used for a wide range of rock mechanical issues, there is some primary restriction associated with using PBM. For example, one of the fundamental limitations of conventional bonding models (CBM and PBM) is an unrealistically low uniaxial compressive strength to tensile strength ratio in the range of 3–7 (Potyondy and Cundall 2004).

Several research works have been done to overcome the limitation and proposed some different models compared to the linear models. Potyondy and Cundall (2004) suggested clustering the circular disks which are defined as a set of particles that are adjacent to one another. In clustered assemblies, particles are modeled as a group of individual circular disks. Cho *et al*. (2007) showed that controlling the properties of particles had a low effect on the macro mechanical properties of uniaxial compressive and tensile strength tests, but using a clumped-particle geometry improves the predictive abilities of the particle code remarkably. Potyondy (2010) emphasized the interlocking of the grains and suggested a polygonal grain structure or grain-based model to overcome the difference between simulations and experimental results of Äspö diorite rock subjected to uniaxial compressive and direct tension tests.

Potyondy (2012) proposed a flat-joint bonded model that behavior of a finite-length interface between two disks is simulated by each disk-disk contact like parallel bond models. However, the flat joint model can successfully simulate a brittle rock with the compressive strength to tensile strength ratio within a range of 24.

A flat-joint model consists of bodies (balls, clumps, or walls) bonded by flat-joint contacts which the effective surface of each body is defined by the notional surfaces of these pieces interacting at each flat-joint contact with a notional surface of the contacting piece (Potyondy 2013). Fig. 8 shows a schematic diagram of a flat joint contact and flat joint material.

The major advantage of the flat joint bonded model compared to the conventional bonded model is to simulate sectional interface damage and continued moment-resisting ability. In the flat-joint model, the interface is divided into small segments and all the segments are connected by default. When the bonded segments break due to the loading, the interface behavior alters from a bonded mode to a frictional mode. After completely breaking, the interface can resist relative rotation; however, in the breaking of the parallel bond model, interface behavior decays to a zero-length interface (Potyondy 2013). Fig. 9 schematically illustrates partial damage of the flat joint model.

As it was mentioned previously, the contact and parallel

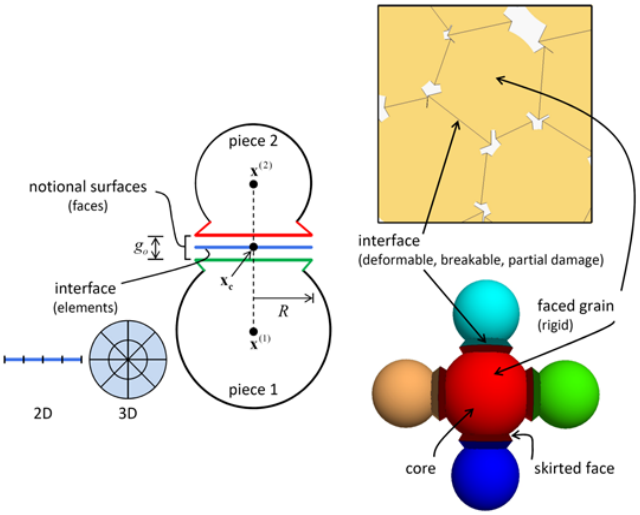

Fig. 8 Flat-joint contact (left) and flat-jointed material (right) (Potyondy 2013)

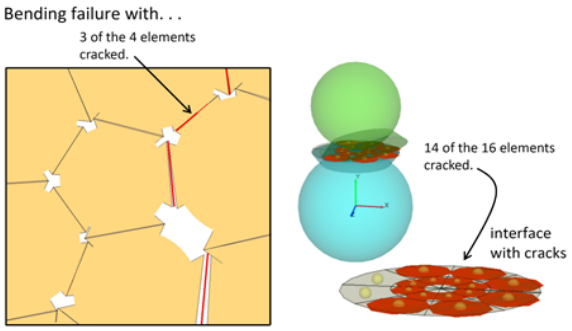

Fig. 9 Partially damaged flat-jointed material showing faced grains with cracks colored red/blue for tensile/shear failure (Potyondy 2013)

Table 4 Comparison between standard BPM and flat joint model (Wu and Xu 2016)

Standard BPM	Flat Joint Model
Interface vanishes after breaking	Interface still exists
Entire interface breaks	Each element breaks
Element: deformable, Breakable	Element: deformable, partially damaged, breakable
cannot resist rotation after breaking	can resist rotation after breaking

bond particle models are not able to simulate the high ratio of compressive to tensile strength that the flat joint model has coped with this concern. The differences between the flat joint model and standard bond particle model (PBM and CBM) are summarized in Table 4.

5.2 Preparation and calibration of the numerical model

Generally, model generation in PFC2D involves two main stages: generation of geometry and applying the bonded model. The material generation process begins with the creation of a rectangular vessel consisting of planar frictionless walls with the same dimensions as the laboratory test sample, and an assembly of disks is generated to fill the vessel. The model has solved to a dense-packed circular disk and then flat-joint model is applied by bonding all contacts between circular particles. The particle size cannot be chosen arbitrarily as it can be an effective parameter to compare the results of numerical simulation with the results of experimental tests.

Practically, all of the mechanical properties of numerical modeling such as compressive strength, tensile strength, and young modulus are heavily influenced by the size particles.

Numerical models need to be calibrated. For this, in such a calibration procedure, a set of micro-parameters must be defined to get the desired macro-parameters. In other words, the micro-parameters of the numerical model in PFC2D can be calibrated based on the macro-parameters, e.g., UCS, Poisson's ratio, Young's modulus, and tensile strength. Since the micro-parameters cannot be measured directly with experimental tests, they have to be calibrated based on the results of experimental tests. This calibration procedure is called the "trial and error" method. A systematic calibration procedure was established to minimize the number of iterations. First, the calibration process started with the elastic constant. The Young modulus was adjusted by changing the elastic modulus of the flat-joint contacts. Second, Poisson's ratio should be calibrated so that this parameter was determined by varying the ratio of the contact normal to shear stiffness. Both values were calibrated after a few iterations. Third, the flat joint contact tensile strength and cohesion parameters were changed to get the desired values of uniaxial compressive and Brazilian tensile strength.

In this study, after geometry generation and installation of bonding model, results of the uniaxial compressive test and Brazilian test were used to calibrate the micro-properties of particles and flat-joint bonding model. For this purpose, the experimental tests of uniaxial compression were simulated in PFC2D and an appropriate set of micro-parameters were determined by trial and error process to get desired macro-parameters.

Table 5 Micro parameter obtained through the calibration process

Micro parameters (unit)	Rock-like plaster	Sandstone	Granite
Density $\left(\frac{kg}{m^3}\right)$	1000	2770	2900
Porosity (%)	8	2	2
Damping coefficient	0.7	0.1	0.1
Minimum diameter (mm)	0.54	0.3	0.3
Size ratio	1.66	1.66	1.66
Effective elastic modulus (GPa)	3.5	38	57
Normal to shear stiffness ratio	1.7	3.2	3.4
Friction coefficient	0.4	0.5	0.5
Tensile strength mean (MPa)	1.75	23	21
Tensile strength S.D. (MPa)	1	13	12
Cohesion strength mean (MPa)	1.75	86	133
Cohesion strength S.D. (MPa)	1	35	50

The uniaxial compression test can be generated as a model with two moving walls which compress the densely packed particles. In this study, the height and width of the generated model are 108 mm and 54 mm, respectively. During the test, the value of vertical forces acting on the boundaries and their displacements are recorded. Consequently, Young's modulus and Poisson's ratio of the specimen can be calculated for the linear portion of the stress-strain curve at 50% of ultimate strength.

The value of tensile strength in the numerical model was calibrated with the simulation of an indirect (Brazilian) tensile strength test. To this end, the Brazilian specimen model was generated in PFC2D, and then, a vertical compression force was applied to the specimen by moving the platens toward each other. During the numerical simulation, the force acting on the walls is recorded, and the maximum value corresponding to the failure point is obtained to measure the indirect tensile strength of the specimen by

$$\sigma_t = \frac{2F_{max}}{\pi D} \tag{1}$$

Where F_{max} is the maximum axial force at the failure point, and D is the diameter of the Brazilian disk specimen. It should be considered that the simulated models in the PFC2D have a unit thickness.

Table 5 represents all the micro-parameters of the flat-joint bonded model obtained through the calibration process for three rock types with different brittleness. The calibrated models showed a good agreement between the experimental tests and numerical results which can be seen in Tables 6, 7, and 8.

Table 6 Macro-mechanical properties of the rock-like plaster in the experimental tests and PFC2D models

Properties (unit)	Experimental results	PFC2D model results
UCS (MPa)	6.6	6.7
Elastic modulus (GPa)	5	4.8
Poisson's ratio	0.18	0.17
Tensile strength (MPa)	1	0.95

Table 7 Macro-mechanical properties of the Sandstone in the experimental tests and PFC2D models

Properties (unit)	Experimental results	PFC2D model results
UCS (MPa)	159.13	158
Elastic modulus (GPa)	39.63	39.47
Poisson's ratio	0.17	0.16
Tensile strength (MPa)	11.58	11.7

Table 8 Macro-mechanical properties of the Granite in the experimental tests and PFC2D models

Properties (unit)	Experimental results	PFC2D model results
UCS (MPa)	224	226
Elastic modulus (GPa)	60	59.5
Poisson's ratio	0.2	0.19
Tensile strength (MPa)	10	10.1

6. Influence of rock brittleness on rock failure mechanism

Based on the aforementioned discussion, the flat-joint model is able to simulate the high ratio of compression uniaxial strength to Brazilian tensile strength. The ability to calibrate rock samples with different brittleness is the most significant feature of the current bond particle model. According to previous studies, the conventional bond particle models (CBM and PBM) were not able to simulate these types of rock. Additionally, the other operational parameters such as the stress-strain curve, the number of tensile and shear cracks can be considered simultaneously through the study of the brittleness effect on the failure mechanism. Fig. 10 shows the variations of shear and tensile cracks number versus strain during the uniaxial compression test in addition to the stress-strain curve as a reference. In this section, the behavior of rock-like plaster specimens has been investigated in four stages:

(1) S25 means the value of stress at 25% of peak strength,
(2) S50 means the value of stress at 50% of peak strength,
(3) S75 means the value of stress at 75 % of peak strength,
(4) S100 means peak strength.

Table 9 Number of shear crack, tensile crack, and strain value in four stages of fracture process

Values designation	S25	S50	S75	S100
Shear crack number	1557	4721	8923	16417
Tensile crack number	199	501	1240	4100
Axial strain (%)	0.031	0.062	0.095	0.143

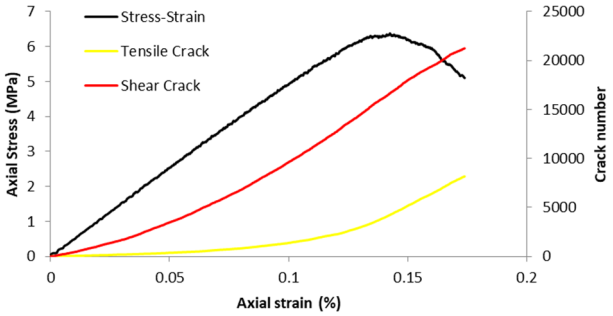

Fig. 10 Stress-strain curve for rock-like plaster specimen in UCS test, the number of tensile and shear cracks during the increase of axial strain

Moreover, the values of shear and tensile cracks plus strain can be found in Table 9. According to Table 9 and Fig. 10, a small number of cracks can be sensed at the beginning of the loading sequence. Since the specimen was in the crack initiation stage, the augmentation of the cracks was gradual up to nearly the S50 stage. After this stage, the growth of cracks accelerated which corresponds to crack damage stress. When the S75 was left behind, the number of shear cracks increased as the model reached the stage taking place numerous shear and tensile cracks due to damage stress. Finally, the curves stretched to the S100 with the peak strength of 6.6 MPa which showed a good agreement with the experimental test. The final failure of the specimen is associated with an abrupt increase in the rate of micro-cracking dealing with the formation of the macro-failure surface across the specimen. Subsequently, the cracks showed cumulative behavior after the post-peak. It can be concluded that the shear cracks perform a chief role in the failure of low brittle rock types. Also, it is worth mentioning that the stress-strain curve in low brittle rock types decreased steadily, contrary to high brittle rock types showing a sudden drop.

As mentioned earlier, in low brittle rocks, the number of shear cracks is more than the number of tensile cracks in this rock type; hence, it seems that the shear cracks play the main role in the failure process of low brittle rock types. Based on previous studies, plastic deformation can be attributed to shear crack behavior. Also, increasing of shear crack results in widening of plastic deformation. Thus, plastic deformation and the value of axial strain in low brittle rock types originate from shear crack. Researchers such as Nejati and Ghazvinian (2014) and Nazerigivi *et al.* (2018) have conducted projects showing that the low brittle materials have a large plastic deformation and an excessive number of shear cracks.

The fracture process of sandstone (brittle) indicated

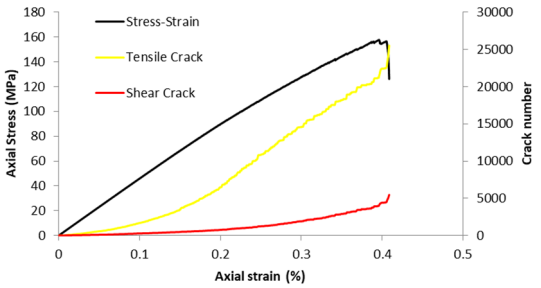

Fig. 11 Stress-strain curve for Sandstone specimen in UCS test, the number of tensile and shear cracks during the increase of axial strain

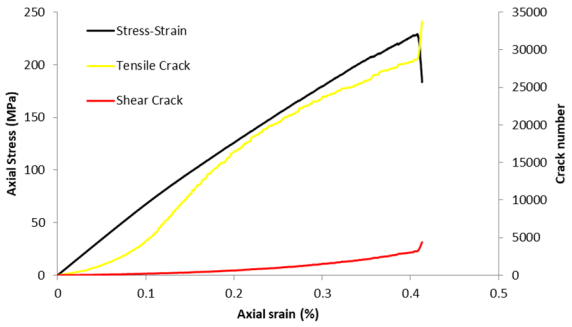

Fig. 12 Stress-strain curve for Granite specimen in UCS test, the number of tensile and shear cracks during the increase of axial strain

Table 10 Number of shear crack, tensile crack, and strain in four stages of failure process

Values designation	S25	S50	S75	S100
Shear crack number	234	615	1564	4095
Tensile crack number	1321	4955	12818	21415
Axial strain (%)	0.08	0.17	0.27	0.39

Table 11 Number of shear crack, tensile crack, and strain in four stages of failure process

Values designation	S25	S50	S75	S100
Shear crack number	158	496	1269	3006
Tensile crack number	3132	13896	22450	28346
Axial strain (%)	0.09	0.18	0.27	0.4

different behavior in comparison with rock-like plaster (low brittle). It can be seen by Fig. 11 and Table 10 that a small number of cracks were generated at the beginning of the loading sequence and the number of cracks showed a slow increase until 0.1% of axial strain. Tensile crack types were dominant in the sandstone specimen, nonetheless, shear crack types appeared once the stress reached nearly to S50. Following this stage, the growth of cracks up to failure point hastened relating to crack damage stress. Also, the majority of shear cracks arose near peak strength point which is related to the failure of the model. It can be concluded that in this kind of brittle rock type, the small number of shear cracks caused the small plastic deformation.

As a final point, the preceding values and curves of tensile and shear cracks for the Granite rock can be found in Fig. 12 and Table 11. Similar behavior of failure process seems between granite and sandstone. The total number of cracks increases by increasing the ratio of UCS/BTS because the high rate shows more brittle behavior. Likewise, the high brittle rock types absorb more strain energy causing further tensile cracks in the specimen; therefore, the stress-strain curve, in this case, drops immediately after reaching to the failure point.

Moreover, based abovementioned discussion about crack behavior in brittle and high brittle rock types which show more tensile cracks, in this regard, the bond cannot tolerate the loading because of eliminating resistance and

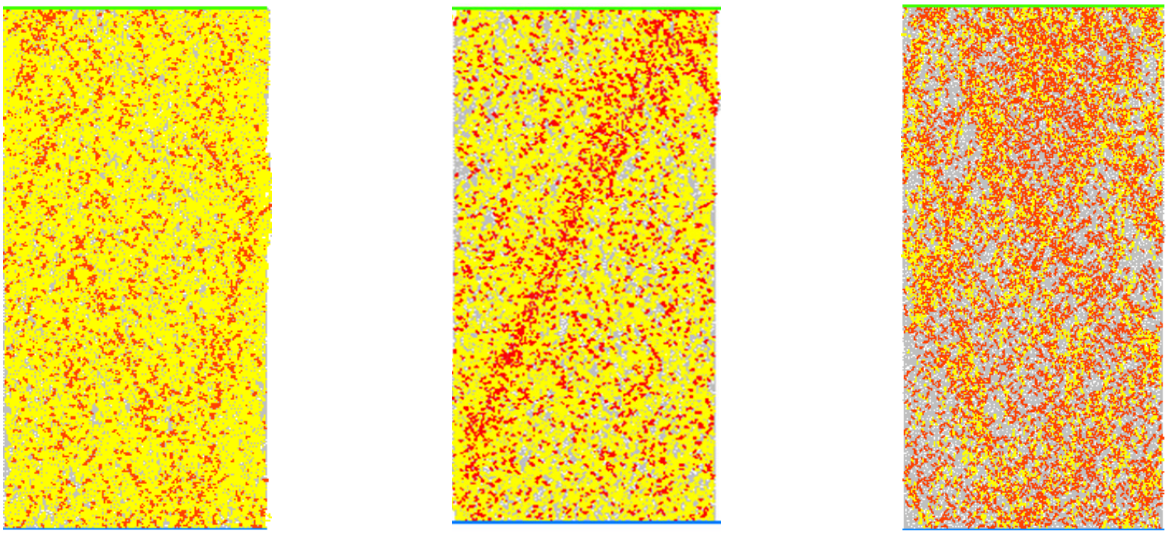

(a) High-Brittle (b) Semi-Brittle (c) Low-Brittle

Fig. 13 Numerical failure pattern of specimens

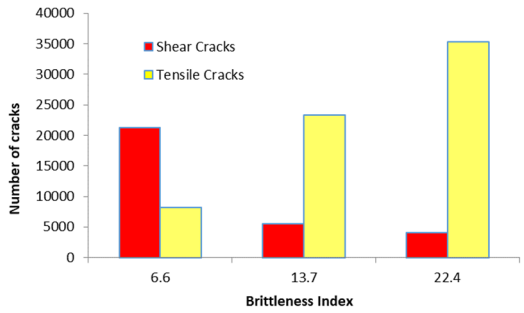

Fig. 14 The number of cracks in different brittleness

the presence of tensile cracks which cause the stress-strain curve to drop vertically. In contrast, in low-brittle rocks, bonds still endure the loading due to active friction among bonds and the nature of shear cracks when each bond fails. Correspondingly, the value of plastic deformation in high brittle rock types is less in comparison to brittle ones.

As mentioned before, induced micro-cracks on the specimens during the loading sequences influence on the macro-failure mode of the specimens. Fig. 13 illustrates the numerical failure modes of the three selected specimens. As shown in Fig. 13(a) many tensile micro-cracks which oriented parallel to the loading direction formed in the high-brittle specimen. Also, a shearing failure mode was detected in the semi-brittle specimen (Fig. 13(b)) and finally, Fig. 13(c) shows that shear cracks are the predominant fractures in the low-brittle specimen.

The variation of the number of tensile and shear cracks in different rock types with dissimilar brittleness is given in Fig. 14. It can be seen that the number of tensile cracks in low-brittle rock types is less than in semi-brittle and high-brittle ones. Because plastic deformation stems from the shear cracks in low-brittle rock types, most of the strain energy consumes by plastic deformation rather than creating a new failure plane; for that reason, the number of tensile cracks is less than brittle and high-brittle rock types. In brittle rock types, not much plastic deformation occurs and most of the strain energy consumes through creating a new failure plane so that numerous tensile cracks turn on in this concern. As a consequence, the tensile cracks have a controlling influence on brittle and high brittle rock types. Thereby, the failure modes and pattern can be influenced by the type of cracks so that the failure process is deeply affected by the majority of shear and tensile cracks. The different ratio of brittleness leads to different failure mechanisms in compression tests.

Furthermore, a model with a low ratio of brittleness fails in ductile mode with more shear cracks at the point of peak strength, while a high ratio of brittleness model fails in brittle mode occurring more tensile cracks, as it was shown in Fig. 14. In the current work, the ratio of tensile crack to shear crack numbers were 0.3, 4.82, and 9.87 when the ratio of UCS/BTS was set to 6.6, 13.74, and 22.4, respectively.

7. Conclusions

In the present study, effect of brittleness on crack evolution of rock specimens was investigated using experimental and numerical modeling. The ratio of $BI = \frac{\sigma_c}{\sigma_t}$ was considered as brittleness index and failure mechanism of rock specimens was assessed over a wide range of brittleness (6.6-22.4). However, the selected specimens categorized in three different groups of (1) Low-brittle: BI < 9, (2) Semi-brittle: 9 < BI < 15, and (3) High-brittle: BI > 15.

Results of experimental tests indicated that three macro-failure patterns are detectable for all of the three mentioned studied specimens: low-brittle specimens failed in spalling-shearing mode, while the specimens with semi-brittleness possess shearing macro-failure. Furthermore, the failure mode of the specimens with high brittleness is the tensile axial splitting mode.

The number of shear cracks is more than the number of tensile cracks in the low brittle rock types; hence, it seems that the shear cracks play the main role in the failure process of low brittle rock specimens.

Tensile micro-cracks were dominant in the semi-brittle specimens, nonetheless, shear micro-cracks appeared once the stress reached nearly 50 percent of peak strength and the macro failure pattern of the semi-brittle specimens was influenced by the shear micro-cracks.

The number of tensile micro-cracks in high brittle specimens significantly increases during the loading sequences compared to the low- and semi-brittle specimens. The failure mode is heavily influenced by the type of induced cracks; therefore, the macro failure pattern of high brittle specimens was affected by numerous tensile micro cracks which oriented parallel to the loading direction.

The total number of cracks increases by increasing the brittleness index. Likewise, the high brittle rock types absorb more strain energy causing further tensile cracks in the specimen; therefore, the stress-strain curve, in this case, drops immediately after getting to the failure point.

References

Aggelis, D.G., Soulioti, D.V., Sapouridis, N., Barkoula, N.M., Paipetis, A.S. and Matikas, T.E. (2011), "Acoustic emission characterization of the fracture process in fibre reinforced concrete", *Constr. Build. Mater.als*, **25**, 4126-4131. https://doi.org/10.1016/j.conbuildmat.2011.04.049

Aggelis, D.G., Mpalaskas, A.C. and Matikas, T.E. (2013), "Acoustic signature of different fracture modes in marble and cementitious materials under flexural load", *Mech. Res. Commun.*, **47**, 39-43. https://doi.org/10.1016/j.mechrescom.2012.11.007

Altindag, R. (2000), "The role of rock brittleness on analysis of percussive drilling performance", *Proceedings of 5th National Rock Mechanics Symposium*, Turkey, pp. 105-112. [In Turkish]

Asadizadeh, M., Babanouri, N., Nowak, S. and Sherizah, T. (2021), "The evolution of dynamic energy during drop hammer testing of Brazilian disk with non-persistent joints: an extensive experimental investigation", *Theor. Appl. Fract. Mech.*, p. 103162. https://doi.org/10.1016/j.tafmec.2021.103162

Basu, A., Mishra, D.A. and Roychowdhury, K. (2013), "Rock failure modes under uniaxial compression, Brazilian, and point load tests", *Bull. Eng. Geol. Environ.*, **72**(3-4), 457-475. https://doi.org/10.1007/s10064-013-0505-4

Bieniawski, Z.T. (1967), "Mechanism of brittle fracture of rock. Part II — experimental studies", *Int. J. Rock Mech. Min. Sci.*

Geomech. Abstr., **4**(4), 407-423. https://doi.org/10.1016/0148-9062(67)90031-9

Blindheim, O.T. and Bruland, A. (1998), "Boreability testing, Norwegian TBM tunnelling 30 years of Experience with TBMs in Norwegian Tunnelling", Norwegian Soil and Rock Engineering Association, Publication, pp. 29-34.

Bobet, A. and Einstein, H.H. (1998), "Fracture coalescence in rock type materials under uniaxial and biaxial", *Int. J. Rock Mech. Min. Sci.*, **35**(7), 863-888. https://doi.org/10.1016/S0148-9062(98)00005-9

Cai, M. and Liu, D. (2009), "Study of failure mechanisms of rock under compressive – shear loading using real-time laser holography", *Int. J. Rock Mech. Min. Sci.*, **46**, 59-68. https://doi.org/10.1016/j.ijrmms.2008.03.010

Cai, M., Kaiser, P.K., Suorineni, F. and Su, K. (2007), "A study on the dynamic behavior of the Meuse/Haute-Marne argillite", *Physics and Chemistry of the Earth*, *Parts A/B/C*, **32**(8-14), 907-916. https://doi.org/10.1016/j.pce.2006.03.007

Chen, G., Li, T., Wang, W., Guo, F. and Yin, H. (2017), "Characterization of the brittleness of hard rock at different temperatures using uniaxial compression tests", *Geomech. Eng., Int. J.*, **13**(1), 63-77. https://doi.org/10.12989/gae.2017.13.1.063

Chen, S.J., Ren, M.Z., Wang, F., Yin, D.W. and Chen, D.H. (2020), "Mechanical properties and failure mechanisms of sandstone with pyrite concretions under uniaxial compression", *Geomech. Eng., Int. J.*, **22**(5), 385-396. http://doi.org/10.12989/gae.2020.22.5.385

Cho, N.A., Martin, C.D. and Sego, D.C. (2007), "A clumped particle model for rock", *Int. J. Rock Mech. Min. Sci.*, **44**(7), 997-1010. https://doi.org/10.1016/j.ijrmms.2007.02.002

Dursun, A.E. and Gokay, M.K. (2016), "Cuttability assessment of selected rocks through different brittleness values", *Rock Mech. Rock Eng.*, **49**(4), 1173-1190. https://doi.org/10.1007/s00603-015-0810-2

Fakhimi, A. and Hemami, B. (2015), "Axial splitting of rocks under uniaxial compression", *Int. J. Rock Mech. Min. Sci.*, **79**, 124-134. https://doi.org/10.1016/j.proeng.2017.05.226

Fan, L.F., Wu, Z.J., Wan, Z. and Gao, J.W. (2017), "Experimental investigation of thermal effects on dynamic behavior of granite", *Appl. Thermal Eng.*, **125**, 94-103. https://doi.org/10.1016/j.applthermaleng.2017.07.007

Fan, L., Gao, J., Du, X. and Wu, Z. (2020), "Spatial gradient distributions of thermal shock-induced damage to granite", *J. Rock Mech. Geotech. Eng.*, **12**(5), 917-926. https://doi.org/10.1016/j.jrmge.2020.05.004

Fan, L.F., Yang, K.C., Wang, M., Wang, L.J. and Wu, Z.J. (2021), "Experimental study on wave propagation through granite after high-temperature treatment", *Int. J. Rock Mech. Min. Sci.*, **148**, 104946. https://doi.org/10.1016/j.ijrmms.2021.104946

Gao, J., Xi, Y., Fan, L. and Du, X. (2021), "Real-time visual analysis of the microcracking behavior of thermally damaged granite under uniaxial loading", *Rock Mech. Rock Eng.*, **54**(12), 6549-6564. https://doi.org/10.1007/s00603-021-02639-0

Ghazvinian, A., Nejati, H.R., Sarfarazi, V. and Hadei, M.R. (2013), "Mixed mode crack propagation in low brittle rock-like materials", *Arab. J. Geosci.*, **6**(11), 4435-4444. https://doi.org/10.1007/s12517-012-0681-8

Gong, Q.M. and Zhao, J. (2007), "Influence of rock brittleness on TBM penetration rate in Singapore granite", *Tunnell. Undergr. Space Technol.*, **22**(3), 317-324. https://doi.org/10.1016/j.tust.2006.07.004

Gramberg, J. (1989), *A Non-conventional View on Rock Mechanics*, Rotterdam: Balkema.

Haeri, H. and Marji, M.F. (2016), "Simulating the crack propagation and cracks coalescence underneath TBM disc cutters", *Arab. J. Geosci.*, **9**(2), 124. https://doi.org/10.1007/s12517-015-2137-4

Heidari, M., Khanlari, G.R., Torabi-Kaveh, M., Kargarian, S. and Saneie, S. (2014), "Effect of porosity on rock brittleness", *Rock Mech. Rock Eng.*, **47**(2), 785-790. https://doi.org/10.1007/s00603-013-0400-0

Hoek, E. and Bieniawski, Z.T. (1965), "Brittle fracture propagation under compression", *Int. J. Fract. Mech.*, **1**, 137-55. https://doi.org/10.1007/BF00186851

Hucka, V. and Das, B. (1974), "Brittleness determination of rocks by different methods", *Int. J. Rock Mech. Min. Sci. Geomech. Abstracts*, **11**(10), 389-392. https://doi.org/10.1016/0148- 9062(74)91109-7

Imani, M., Nejati, H.R. and Goshtasbi, K. (2017), "Dynamic response and failure mechanism of Brazilian disk specimens at high strain rate", *Soil Dyn. Earthq. Eng.*, **100**, 261-269. https://doi.org/10.1016/j.soildyn.2017.06.007

ISRM (1981), In: Brown, E.T. (ed.), *Suggested methods*: *rock characterization*, *testing and monitoring*, Pergamon, Oxford, p. 211.

Itasca Consulting Group (2008), PFC2D (particle flow code in 2 dimensions), version 4.0, manual. Minneapolis: ICG.

Jaeger, J.C., Cook, N.G. and Zimmerman, R. (2009), *Fundamentals of Rock Mechanics*, John Wiley & Sons.

Kahraman, S. (2002), "Correlation of TBM and drilling machine performances with rock brittleness", *Eng. Geol.*, **65**(4), 269-283. https://doi.org/10.1016/S0013-7952(01)00137-5

Kahraman, S. and Altindag, R. (2004), "A brittleness index to estimate fracture toughness", *Int. J. Rock Mech. Min. Sci.*, **2**(41), 343-348. https://doi.org/10.1016/j.ijrmms.2003.07.010

Khodayar, A. and Nejati, H.R. (2018), "Effect of thermal-induced microcracks on the failure mechanism of rock specimens", *Comput. Concrete*, *Int. J.*, **22**(1), 93-100. http://doi.org/10.12989/cac.2018.22.1.093

Kim, J.S., Kim, G.Y., Baik, M.H., Finsterle, S. and Cho, G.C. (2019), "A new approach for quantitative damage assessment of in-situ rock mass by acoustic emission", *Geomech. Eng., Int. J.*, **18**(1), 11-20. http://doi.org/10.12989/gae.2019.18.1.011

Lavrov, A. (2003), "The Kaiser effect in rocks: principles and stress estimation techniques", *Int. J. Rock Mech. Min. Sci.*, **40**(2), 151-171. https://doi.org/10.1016/s1365-1609(02)00138-7

Mardalizad, A., Scazzosi, R., Manes, A. and Giglio, M. (2018), "Testing and numerical simulation of a medium strength rock material under unconfined compression loading", *J. Rock Mech. Geotech. Eng.*, **10**(2), 197-211. https://doi.org/10.1016/j.jrmge.2017.11.009

Marji, M.F. (2014), "Numerical analysis of quasi-static crack branching in brittle solids by a modified displacement discontinuity method", *Int. J. Solids Struct.*, **51**(9), 1716-1736. https://doi.org/10.1016/j.ijsolstr.2014.01.022

Marji, M.F. (2015), "Simulation of crack coalescence mechanism underneath single and double disc cutters by higher order displacement discontinuity method", *J. Central South Univ.*, **22**(3), 1045-1054. https://doi.org/10.1007/s11771-015-2615-6

Meng, F., Zhou, H., Zhang, C., Xu, R. and Lu, J. (2015), "Evaluation methodology of brittleness of rock based on post-peak stress– strain curves", *Rock Mech. Rock Eng.*, **48**(5), 1787-1805. https://doi.org/10.1007/s00603-014-0694-6

Mughieda, O.S. and Khawaldeh, I. (2006), "Coalescence of offset rock joints under biaxial loading", *Geotech. Geol. Eng.*, **24**, 985-999. https://doi.org/10.1007/s10706-005-8352-0

Nazerigivi, A., Nejati, H.R., Ghazvinian, A. and Najigivi, A. (2017), "Influence of nano-silica on the failure mechanism of concrete specimens", *Comput. Concrete*, *Int. J.*, **19**(4), 429-434. https://doi.org/10.12989/cac.2017.19.4.429

Nazerigivi, A., Nejati, H.R., Ghazvinian, A. and Najigivi, A. (2018), "Effects of SiO_2 nanoparticles dispersion on concrete fracture toughness", *Constr. Build. Mater.*, **171**, 672-679. https://doi.org/10.1016/j.conbuildmat.2018.03.224

Nejati, H.R. and Ghazvinian, A. (2014), "Brittleness effect on rock fatigue damage evolution", *Rock Mech. Rock Eng.*, **47**(5), 1839-1848. https://doi.org/10.1007/s00603- 013-0486-4

Nejati, H.R. and Moosavi, S.A. (2017), "A new brittleness index for estimation of rock fracture toughness", *J. Min. Environ.*, **8**(1), 83-91. https://doi.org/10.22044/JME.2016.579

Nejati, H.R., Nazerigivi, A., Imani, M. and Karrech, A. (2020), "Monitoring of fracture propagation in brittle materials using acoustic emission techniques-A review", *Comput. Concrete*, *Int. J.*, **25**(1), 15-27. http://doi.org/10.12989/cac.2020.25.1.015

Panaghi, K., Golshani, A. and Takemura, T. (2015), "Rock failure assessment based on crack density and anisotropy index variations during triaxial loading tests", *Geomech. Eng.*, *Int. J.*, **9**(6), 793-813. http://doi.org/10.12989/gae.2015.9.6.793

Park, C.H. and Bobet, A. (2009), "Crack coalescence in specimens with open and closed flaws: A comparison", *Int. J. Rock Mech. Min. Sci.*, **46**, 819-829. https://doi.org/10.1016/j.ijrmms.2009.02.006

Paul, B. (1968), "Macroscopic criteria for plastic flow and brittle fracture", *Fracture*, **2**, 313-496.

Potyondy, D.O. (2010), "A grain-based model for rock: approaching the true microstructure", *Proceedings of Rock Mechanics in the Nordic Countries*, pp. 9-12.

Potyondy, D.O. (2012), "A flat-jointed bonded-particle material for hard rock", *Proceedings of the 46th US Rock Mechanics/Geomechanics Symposium*, American Rock Mechanics Association.

Potyondy, D. (2013), PFC3D Flat-Joint Contact Model (version 1), Itasca Consulting Group, Inc., Minneapolis, MN, USA, Technical Memorandum ICG7234-L, June 25, 2013.

Potyondy, D.O. and Cundall, P.A. (2004), "A bonded-particle model for rock", *Int. J. Rock Mech. Min. Sci.*, **41**(8), 1329-1364. https://doi.org/10.1016/j.ijrmms.2004.09.011

Protodyakonov, M.M. (1962), "Mechanical properties and drillability of rocks", *Proceedings of the 5th Symposium on Rock Mechanics*, University of Minnesota Minneapolis, MN, USA, pp. 103-118.

Protodyakonov, M.M. (1963), "Mechanical properties and drillability of rocks", *Proceedings of the 5th Symposium Rock Mechanics*, University of Minnesota, pp. 103-118.

Ren, X., Chen, J.S., Li, J., Slawson, T.R. and Roth, M.J. (2011), "Micro-cracks informed damage models for brittle solids", *Int. J. Solids Struct.*, **48**(10), 1560-1571. https://doi.org/10.1016/j.ijsolstr.2011.02.001

Sagong, M. and Bobet, A. (2002)," Coalescence of multiple flaws in a rock-model material in uniaxial compression", *Int. J. Rock Mech. Min. Sci.*, **39**, 229-241. https://doi.org/10.1016/S1365-1609(02)00027-8

Stefanov, Y.P. (2008), "Numerical modeling of deformation and failure of sandstone specimens", *J. Min. Sci.*, **44**(1), 64-72. https://doi.org/10.1016/0013-7944(94)00201-R

Szwedzicki, T. and Shamu, W. (1999), "The effect of material discontinuities on strength of rock samples", *Proceedings of Australasian Institute of Mining and Metallurgy*, **304**(1), 23-28.

Villaescusa, E. (2014), *Geotechnical Design for Sublevel Open Stopping*, CRC Press.

Wang, S.Y., Sloan, S.W., Sheng, D.C., Yang, S.Q. and Tang, C.A. (2014), "Numerical study of failure behaviour of pre-cracked rock specimens under conventional triaxial compression", *Int. J. Solids Struct.*, **51**(5), 1132-1148. https://doi.org/10.1016/j.ijsolstr.2013.12.01

Wawersik, W. and Fairhurst, C. (1970), "A study of brittle rock fracture in laboratory compression experiments", *Int. J. Rock Mech. Min. Sci. Geomech. Abstr.*, **7**, 561-575.

Wu, S. and Xu, X. (2016), "A study of three intrinsic problems of the classic discrete element method using flat-joint model", *Rock Mech. Rock Eng.*, **49**(5), 1813-1830. https://doi.org/10.1007/s00603-015-0890-z

Xu, X., Wu, S., Gao, Y. and Xu, M. (2016), "Effects of microstructure and micro-parameters on Brazilian tensile strength using flat-joint model", *Rock Mech. Rock Eng.*, **49**(9), 3575-3595. https://doi.org/10.1007/s00603-016-1021-1

Yarali, O. and Soyer, E. (2011), "The effect of mechanical rock properties and brittleness on drillability", *Scientif. Res. Essays*, **6**(5), 1077-1088. https://doi.org/ 10.5897/SRE10.1004

Yoshikawa, S. and Mogi, K. (1981), "A new method for estimation of the crustal stress from cored rock samples: laboratory study in the case of uniaxial compression", *Tectonophysics*, **74**(3-4), 323-339. https://doi.org/10.1016/0040-1951(81)90196-7

CC